

Article

Adaptability of a Reinforced Concrete Diaphragm Wall Cut by Disc Cutter

Hang Yu, Lei Chen * and Kaixi Peng

School of Rail Transportation, Soochow University, Suzhou 215021, China

* Correspondence: leichen@suda.edu.cn

Abstract: On the background of a subway project in Suzhou City of Jiangsu Province and targeting the engineering difficulty of disc cutters cutting reinforced concrete walls, this paper illustrates the adaptability of a reinforced concrete diaphragm wall cut by disc cutter through conducting related laboratory tests and numerical simulations. When cutting a reinforced concrete diaphragm wall, the cutter should use the low-penetration depth excavation pattern with the depth of the penetration kept within 10 mm/r. In order to keep the torque in a small floating range, the cutterhead driving speed and thrust should be strictly controlled during the cutting period. Three types of fracture surface after the cutting operation, namely, single-side rolling destroy, double-sided rolling destroy, and brittle destroy. The percentage of the length of the cut steel bar smaller than 60 cm can reach 44.2% when the driving parameters of the disc cutter are well regulated. The simulation results show that the deeper the penetration, the more unstable the cutting load. The relationship between the normal force of the disc cutter and the penetration depth was linear, and the trend of the simulated value was comparable with the experimental one, which ensures the rationality of this pattern. The cutter spacing had little impact on the cutting results when it was wider than 80 mm.

Keywords: disc cutter cutting process; laboratory test; reinforced concrete diaphragm wall; driving parameters



check for updates

Citation: Yu, H.; Chen, L.; Peng, K.

Adaptability of a Reinforced Concrete Diaphragm Wall Cut by Disc Cutter. *Sustainability* **2022**, *14*, 16154. <https://doi.org/10.3390/su142316154>

Academic Editor: Maged A. Youssef

Received: 2 November 2022

Accepted: 30 November 2022

Published: 2 December 2022

Publisher's Note: MDPI stays neutral with regard to jurisdictional claims in published maps and institutional affiliations.



Copyright: © 2022 by the authors. Licensee MDPI, Basel, Switzerland. This article is an open access article distributed under the terms and conditions of the Creative Commons Attribution (CC BY) license (<https://creativecommons.org/licenses/by/4.0/>).

1. Introduction

The subway station, the aorta of the city, is a civil air-defense construction and a central form of infrastructure. With the advancements in shield technology, subway tunnels are now mostly built by using the shield method; with the increase in transfer stations, the problem of the shield crossing the wall of the existing station is inevitable. Glass fiber is set aside for the diaphragm wall that has to be crossed at the transfer station [1]. Due to the traffic guiding reform and the fast growth of rail transportation, there has been an issue of unreserved shield cutting reinforced concrete diaphragm walls [2,3]. Moreover, with the encryption of metro lines, the issue will become worse and more challenging. The conventional artificial cleaning barrier method is somewhat costly, labor-intensive, and highly dangerous [4]. However, the direct cutting shield crossings can speed up operations, lower construction costs, and improve engineering safety [5]. It is not only a modernization strategy, but also a sustainable development model.

Concrete that has been reinforced is created by combining two substances that have quite different properties. The steel bars in a mesh structure embedded in concrete interact with one another through surface bonding. The cutting procedure includes cutting reinforced concrete in the core area as well as the plain concrete cover of the reinforced concrete buildings [6]. The steel bars in reinforced concrete constructions makes the cutting operation more difficult. Thus, the main part of the project is the way in which to efficiently cut off steel bars. According to incomplete statistics, the reinforced concrete pile foundations or diaphragm walls have been found in more than 20 subway construction projects in more than 10 Chinese cities [7–11]. The pile foundation is the most typical reinforced

concrete structure in shield tunneling during the excavating process. The strongest grade of concrete is C40, the largest primary reinforcement diameter in the pile is 32 mm, the largest number of cutting piles is 137, the largest cutting pile diameter is 1500 mm, and the longest cutting pile diameter is 48 m. The pile group can essentially be removed during the operation through the transformation of the shield cutter and the reinforcement or underpinning of the pile foundation [12–14]. However, some problems still cannot be solved, such as excessive cutter wear or collapse, reinforced winding cutterhead, and building inclination [15–18].

Only a few projects with good construction conditions adopt the method of direct shield cutting across because the cutting volume of the diaphragm wall is significantly larger than that of the pile foundation and there is a lack of related technical experience. For instance, reinforced concrete diaphragm walls with disc-cutting thicknesses of 60 cm are used at the Civic Center Station on the Subway Line 7 in Hangzhou City of Zhejiang Province. Those walls are overall greatly effective, but there is still a dearth of relevant theoretical research and thorough monitoring data. The inability of cutters to cut materials is what causes the technological bottleneck in shield cutting reinforced concrete. Currently, there is no specific cutter for reinforced concrete, which leads to the enhancement of the shield cutterhead. Hard rock is primarily cut with the disc cutter. The disc cutter rolls ahead on the palm surface while rotating the cutter head under the driving thrust, then squeezes the rock mass until the fracture zone between the cutters penetrates and the rock blocks falls off [19–21]. The normal force and rolling force of the disc cutter on the palm surface is primarily related to the impact of the rock cracking [22–26]. The main part of the engineering risk control is to make sure that the disc cutter can cut reinforced concrete materials by its cutterhead configuration. At the same time, that which can be avoided by adjusting the driving parameters are the problems of low efficiency caused by great slow cutting or high cutter load, as well as excessive wear caused by rapid cutting [27–30].

On the basis of a subway project in Suzhou City, we conducted laboratory tests and a numerical simulation of a disc cutter cutting a reinforced concrete diaphragm wall, and following this discuss the adaptability of the disc cutter cutting a reinforced concrete diaphragm wall. This paper assesses the benefits and drawbacks of disc cutter cutting reinforced concrete diaphragm walls and studies the link between cutter load and driving parameters as well as between driving parameters and cutting impact in order to make recommendations for practical engineering.

2. Engineering Background

The new subway line station in Suzhou City is a transfer station along with two subterranean stations that are built as part of the underground tunnel laying, as indicated in Figure 1. The station structural outsourcing measures 169.5 m in total length, 20.264 m in width for the regular portion, and 24.264 m for the expansion section. The route runs straight through the current subway station. The current station is a 1000 m radius curving one on the second underground floor. They are not orthogonal. A bustling business district surrounds the new station, which is next to a construction-intensive zone. The upline of the shield is unable to avoid the plane's current underground path due to the overall section's environmental limitations. In terms of plane distance, Huachi Street is 1.5 m distance from the upline shield tunnel and 2.3 m away from the downline shield tunnel.

The new tunnel is only 1.6 m away from the existing station floor. In the shield crossing range under the existing station, the horizontal MJS full hall reinforcement is adopted from the end of the station. The shield section conflicts with the 0.6 m thickness wall of the existing station at the undercrossing existing line, as shown in Figure 2. The structure of the diaphragm wall is the composite wall, the joint form is the locking pipe, the concrete strength grade is C 30, and the steel bar is an HRB 335 steel bar with a diameter of 25 mm. The existing station floor is set in a silty sand silty soil layer, and the floor of the new shield tunnel is mainly in a silty sand silty soil layer, a silty clay layer, and a clay layer. The

reinforced concrete diaphragm wall on the south side has the plan to adopt the method of direct crossing of the shield grinding wall.

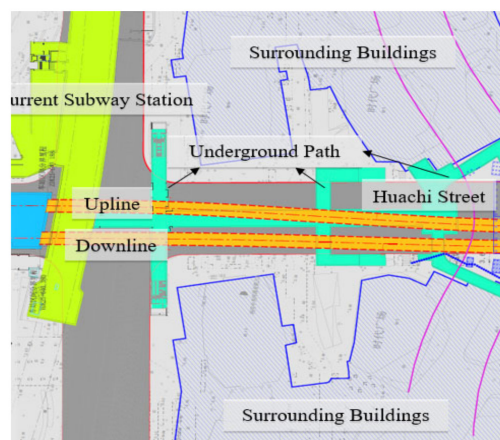


Figure 1. Plan of the project.

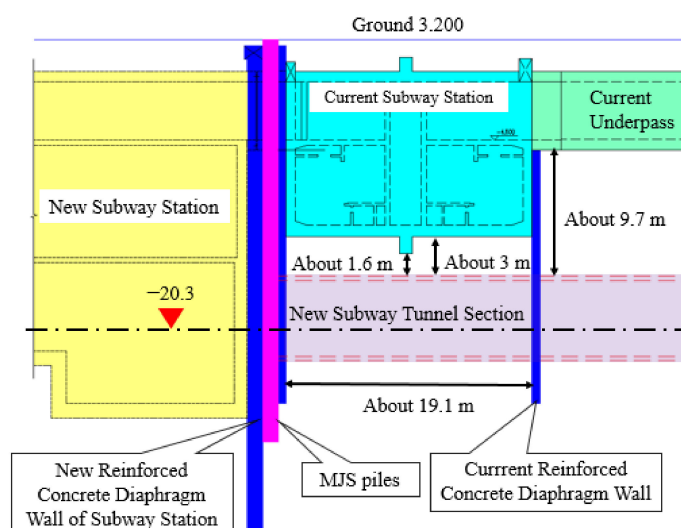


Figure 2. Elevational drawing of the project.

3. Laboratory Test

The interior scale laboratory test of the shield-cutting reinforced concrete diaphragm wall has significant theoretical implications and practical value since it can be used to analyze the test results under varied working situations and inform project design and construction. There are four sets of driving test plans that investigate the failure mode of steel bars, excavation parameters, and cutter force; disclose the failure condition of reinforced concrete under various excavation parameters; and assess the adaptability of cutter cutting reinforced concrete structures.

3.1. Experimental Design

3.1.1. Testing Equipment

The TBM mode driving test bench was used to cut the reinforced concrete diaphragm wall. The size of the test bench was $6880 \times 4050 \times 5176$ mm, the diameter of the cutterhead was 2280 mm, and the equipment torque was 250 kN·m. The cutterhead panel can be installed with three central double disc cutters and eight single disc cutters, and the cutter spacing can be adjusted within the range of 80–100 mm. The test bench can work both horizontally (Figure 3) and vertically.

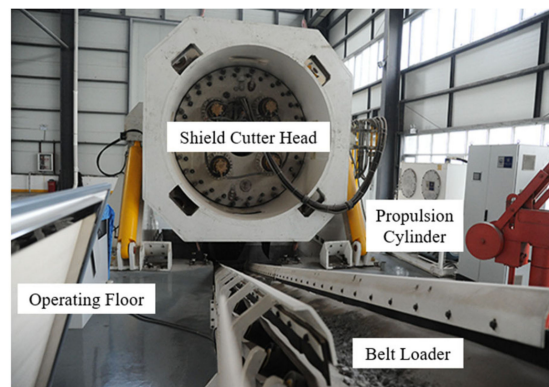


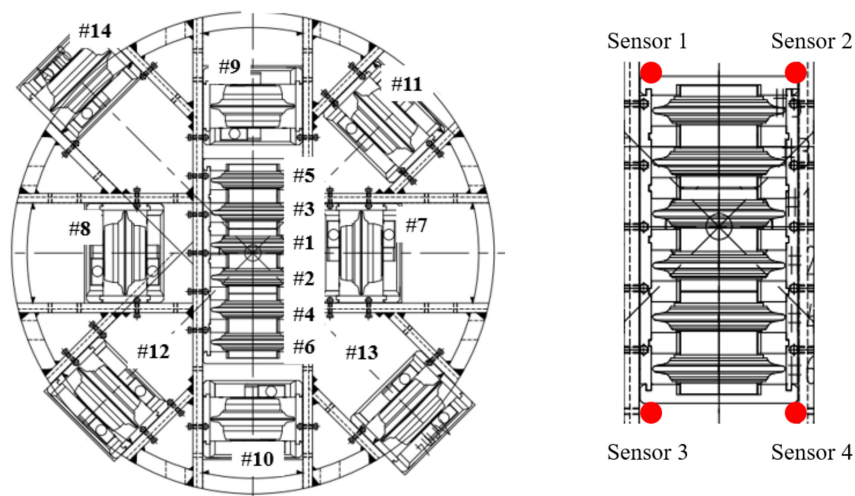
Figure 3. TBM mode driving test bench.

A total of 14 disc cutters with diameters of 432 mm were used in this test, among which cutters No.1 to No.6 were three center double disc cutters with cutter spacings of 84 mm, and cutters No.1 to No.6 were single-disc ones with 100 mm cutter spacing. Each cutter was equipped with wireless sensors for real-time monitoring of each cutter’s typical force. Four sensors were set in each of the No.1 to No.6 center disc cutters, whereas for No.7 to No.14, cutter sensors were set separately. Figure 4 shows the layout of the test cutter, cutterhead configuration, and center disc cutter sensor.



(a) Double-disc cutter

(b) Single-disc cutter



(c) Structural representation of the cutterhead

(d) Center disc cutter sensor layout

Figure 4. Layout of cutterhead configuration and center disc cutter sensor.

3.1.2. Test Sample Preparation

Two layers of reinforced concrete were poured into the rock box mold of the test bench for full disc cutter cutting, and the steel bars were welded on the inner wall of the rock box mold. Each layer of steel mesh consisted of two layers of steel bars with different diameters, in which the transverse steel bars of the steel mesh were set above, and the longitudinal steel bars were below. The transverse steel bar adopted 12 HRB 335 steel bars with diameters of 16 mm and spaces of 200 mm. The longitudinal reinforcement was made up of 16 HRB 335 steel bars with diameters of 25 mm and spaces of 150 mm. C45 concrete was supposed to be poured after the steel mesh was welded. The sample preparation process is shown in Figure 5. The concrete block was retained for compressive test, and the excavation test was conducted after the concrete structure maintenance met the strength requirements.

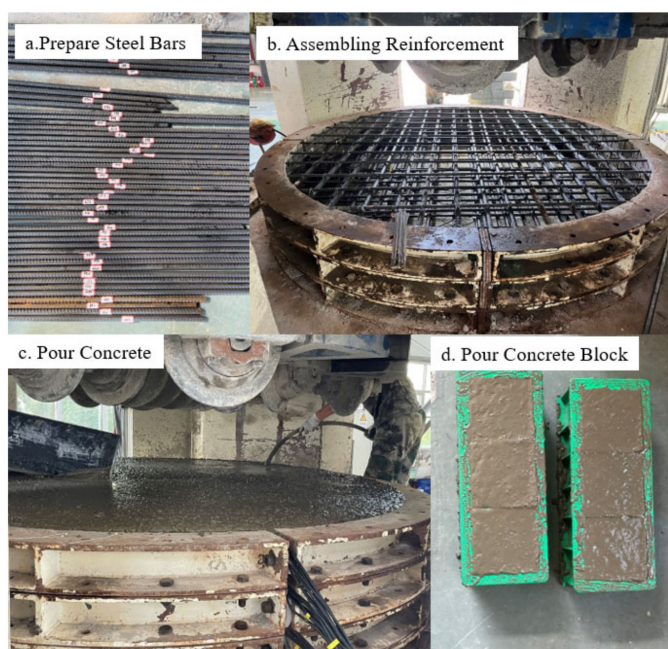


Figure 5. Sample preparation steps.

3.2. Driving Cutting Test

On the basis of the proposed plan, the laboratory test of reinforced concrete structure was carried out, and the two-layer steel mesh was advanced according to different excavation parameters. As shown in Table 1, the test was divided into four parts and obtained four sets of driving parameters. One control group was Part 1 and Part 3, while the other was Part 2 and Part 4.

Table 1. Driving parameters under different working situations.

Part	Cutting Object	Cutterhead Speed/(r/min)	Driving Speed/(mm/min)	Calculate Penetration Depth/(mm/r)
1	16 mm steel reinforcement	2	30	15
2	25 mm steel reinforcement	2	40	20
3	16 mm steel reinforcement	2	40	20
4	25 mm steel reinforcement	2	20	10

We turned the vertical test platform into a horizontal position, launched the propulsion system, and recorded the thrust and torque of the cutterhead in idle condition. The start route and time were also recorded as the cutterhead was pushed to the sample surface at a steady speed. Then, the operator examined the condition of the steel and concrete carefully and activated the belt conveyor to collect the cut steel. The end route and the end time were recorded after the work of each group was finished, and the reinforced concrete wall's structural reaction was accurately evaluated.

3.3. Analysis of Test Cutting Results

3.3.1. Analysis of Disc Cutter Load and Driving Parameters

The cutter sensor data were obtained on the basis of the recording time. Comparison and analysis were conducted on the mean force value of the middle double-disc cutter and the single-disc cutter. The average value of the four measuring points from the six cutters was applied by the center disc cutter. Table 2 displays the mean and maximum number of normal forces of the disc cutter under various working situations.

Table 2. Data of normal force under different working situations.

Number of Disc Cutter	1-0	1-1	2-0	2-1	3-0	3-1	4-0	4-1
Mean/(kN)	123.6	167.1	139.2	163.0	132.5	171.7	92.2	151.28
Maximum/(kN)	149.6	236.8	214.7	278.7	185.5	279.9	174.5	204.6
λ	1.21	1.42	1.54	1.71	1.40	1.63	1.89	1.35

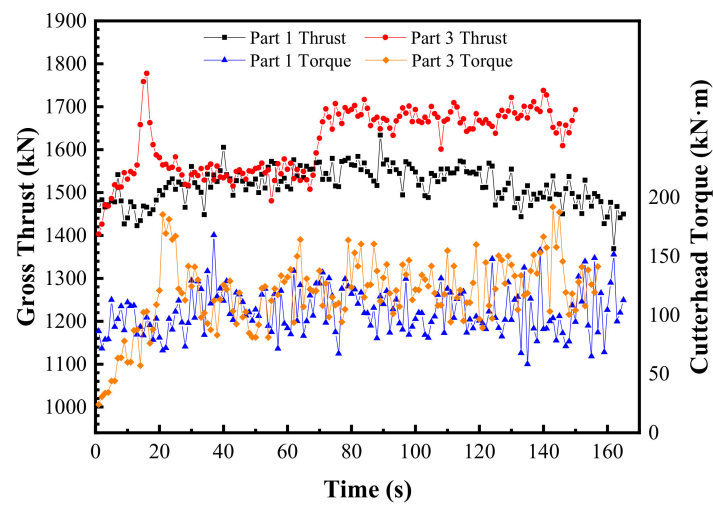
The first number in the disc cutter number represents the working situations: the second number 0 represents the double disc cutter, and 1 represents the single disc cutter; λ = maximum/mean.

The driving parameters of the cutterhead under different working situations are shown in Table 3. The cutterhead speed was kept constant during the tunneling experiment, while the driving speed was changed by input from thrust and torque. As a result, throughout the experiment, the penetration depth changed in real time rather than being a set value. This variation in penetration depth rate with driving speed was referred to as feedback penetration value. The real-time curve of the thrust and torque of the cutterhead under different working situations of Part 1 and Part 3 and Part 2 and Part 4 is shown in Figure 6.

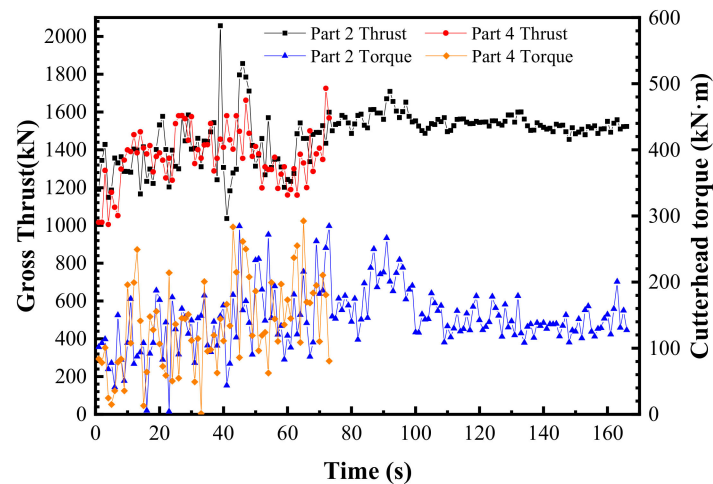
Table 3. Statistics of driving parameters under different working situations.

Part	Footage/(mm)	Actual Penetration Depth/ Feedback Penetration Depth/(mm/r)	Gross Thrust/(kN)		Cutterhead Torque/(kN·m)	
			Mean	Maximum	Mean	Maximum
1	50	15/8	1517	1634	103	168
2	50	20/14	1480	2057	145	285
3	70	20/12	1589	1778	118	192
4	20	10/14	1363	1725	134	292

The driving parameters and cutter load were examined in connection with the test's cutterhead reaction. Comparing working conditions of Part 1 and Part 3 when cutting 16 mm steel bars, what we obtained were as follows: (1) If the cutterhead speed was set to 2 r/min and the driving speed was 30 mm/min (part 1), the cutterhead speed and driving speed matched well, and the thrust and torque also tended to be stable in this situation. This circumstance featured efficient tunneling and smooth cutting. If the driving speed was increased to 40 mm/min (part 3), the thrust and torque of the cutterhead were enhanced in the later stage of cutting, but both of them fluctuated greatly in the early stage. (2) The normal force of the center double-disc cutter was smaller than that of the single one, the λ value of the center double-disc cutter is smaller, and the cutting was more stable.



(a) Thrust and torque at Parts 1 and 3



(b) Thrust and torque at Parts 2 and 4

Figure 6. Thrust and torque under different working conditions.

When comparing working conditions of Part 2 and Part 4 when cutting 25 mm steel bars, what we obtained were as follows: (1) When the cutterhead speed was set to 2 r/min and the driving speed was 40 mm/min (Part 2), it can be seen from Table 2 that the normal force of the inner disc cutter was large and unstable. Figure 6 shows that the thrust and torque fluctuated greatly in the early stage, and there were more peaks. At this time of the excavation process, the phenomenon of machine jamming occurred, and thus the cutting effect was not ideal. When the speed was reduced to 20 mm/min (Part 4), the matching condition between the propulsion speed and the cutterhead speed during the tunneling process was not ideal, resulting in the excessive penetration feedback value, as well as the equivalence of the average value of the disc cutter penetration feedback and the working condition of Part 2. The thrust and torque were still in large fluctuations. (2) In Part 2, the λ value of the whole disc cutter was larger than 1.5, and the cutting process was extremely unstable, which was the cause of the cutterhead jamming. The load of the central double-disc cutter in Part 4 was small, namely, $\lambda = 1.89$; the load of the single-disc cutter was similar to that of Part 2, namely, $\lambda = 1.35$. All of these were due to the unstable driving parameters of this part, which led to most of the steel bar winding cutterhead, and the steel bar was stuck in the central disc cutter. The central disc cutter spent most energy in cutting

concrete in the later period, while the surrounding single disc cutter rolled the twisted steel bar due to the loss of restraint, resulting in a large cutter load throughout the process.

In conclusion, the low penetration depth was supposed to be adopted when the disc cutter cut the reinforced concrete diaphragm wall. To control the cutterhead tunneling speed and thrust, the penetration depth should be kept within 10 mm/r. The torque should be in a restricted range. The cutterhead phenomena can be reversed when the rebar sticks to the cutter head. In terms of a reinforced concrete diaphragm wall structure, the disc cutter's tunneling torque and wear is typically low, which promotes stratum stability and lowers the risk posed by stratum disturbance. The diaphragm wall, which has the thickest concrete layer in actual engineering, can be tunneled through with the disc cutter, which has exceptional tunneling capabilities.

3.3.2. Analysis of Steel Bar Damage Form

According to the analysis of the collected steel bar fracture form, the steel bar fracture can be divided into three types, as shown in Figure 7. The first type is single-sided rolling damage (Figure 7a–c). The surface of the Section a fracture was smooth, namely, a “V” shape section formed by the steel bars fixed at both ends, well constrained with concrete after multiple rolling by disc cutters. The term “reinforcement constraint” refers to both the restriction at the reinforcement's ends and the constraint behind it. The steel bar was pushed by the disc cutter at various angles, and the side was repeatedly sliced until the steel bar broke. The fracture was the most ideal one for disc cutter cutting steel bars. This type also fully displays that it is feasible for a disc cutter to cut steel bars, namely, as long as the steel bars are well constrained, the disc cutter can cut the steel bars smoothly. Section b had thin and flat warping with obvious marks of being rolled by the disc cutter. With the increase in the cutting depth of the disc cutter, the remaining thinned part of the steel bar after rolling was fractured by brittle bending at one time. Section c was a stepped slope with rolling marks and a certain thickness. This fracture was formed by the fracture of the disc cutter after being rolled in the same direction, and brittle fracture occurred when the disc cutter was rolled to nearly half of the steel bar. For the formation of the first type of fracture, what steel actually requires is great boundary constraints.

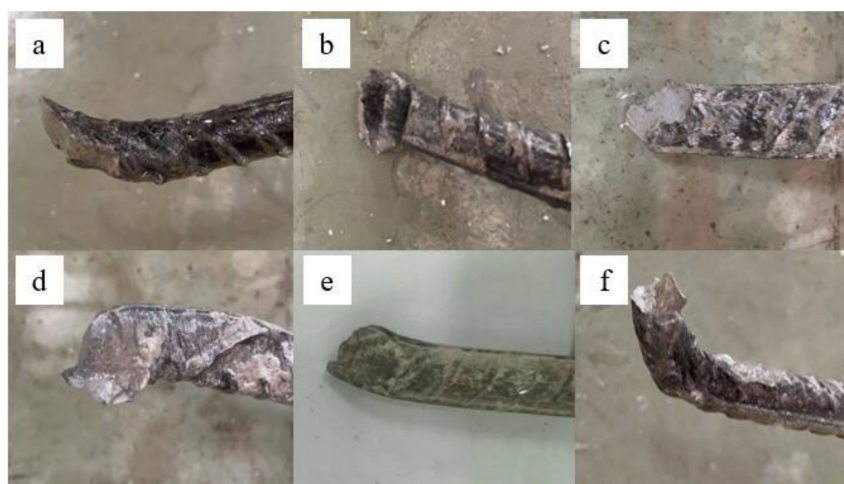


Figure 7. Damage pattern of steel reinforcement. (a) first type of single-sided rolling damage; (b) second type of single-sided rolling damage; (c) third type of single-sided rolling damage; (d) first type of double-sided rolling failure; (e) second type of double-sided rolling failure; (f) brittle failure.

The second type was a double-sided rolling failure (Figure 7). There were some rolling marks on both sides of the fracture, and the middle was thin and the section was flat. The steel bar rotated after being rolled on one side and was rolled by a disc cutter on the other side. According to the degree of rolling, the fracture was divided into two kinds: thin (Figure 7d) and thick (Figure 7e). The steel bar with this fracture is easy to twist. These two

fractures occurred when the steel bar lost concrete confinement. One section of the steel bar was constrained while the other section was not. A certain point was left by the rolling of the disc cutter with the indentation left but the steel bar not cut off, and the unconstrained section of the rebar was warped and bent. When the disc cutter rolled the steel bar for the second time, the rebar twisted under the influence of the cutter head, and the rolling point of the disc cutter changed. At the same time, the indentation was left at the new point of the steel bar by the hob, and the rebar eventually broke under the repeated rolling of the disc cutter.

The third type was brittle failure (Figure 7f). The fracture was high on both sides and low in the middle, and there was no disc cutter rolling mark nearby. Under the action of disc cutter cutting, the surface concrete peeled off and the steel bar was exposed to the surface, and the steel bar was bent and deformed after being rolled by the disc cutter. The steel bar in contact with the disc cutter was compressed, the back was pulled, and stress concentration occurred. The steel bar without restraint bounced back many times after compression and became hard and brittle, finally producing brittle failure.

In this paper, only the steel bars of the fracture caused by the disc cutter were analyzed. The steel bars pulled out by the cutterhead due to poor welding can be considered invalid data. For the reason that the welding effect of the steel bar with the diameter of 16 mm was better than that of steel bar with a diameter of 25 mm, the different lengths of the cut steel bar under Part 1 and Part 3 were statistically analyzed. The results are shown in Table 4 and Figure 8.

Table 4. Statistics of steel reinforcement cut by disc cutter under different parts.

Part	1		3	
Length of Steel Reinforcement/cm	Number of Steel Reinforcement	Proportion/%	Number of Steel Reinforcement	Proportion/%
≤30	10	19.2%	2	4.4%
31~60	13	25%	6	13.0%
61~80	16	30.8%	15	32.6%
81~100	5	9.6%	12	26.1%
>100	8	15.4%	11	23.9%

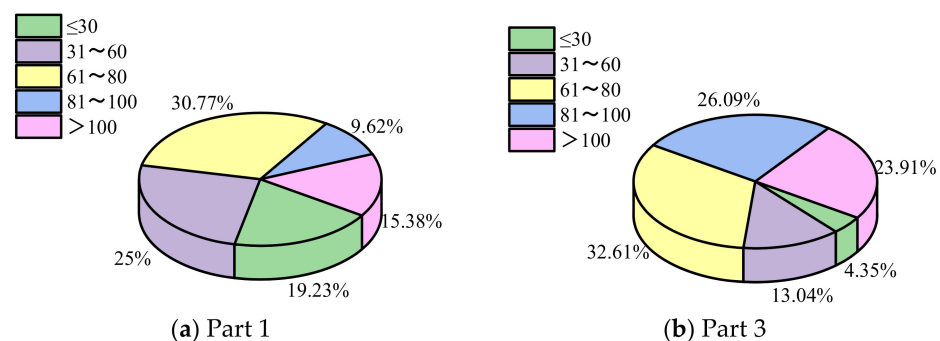


Figure 8. Ratio of steel reinforcement length cut by disc cutter under different parts.

Table 4 and Figure 8 show that the ratio of Part 1 to the total number of steel bars with a length of less than 60 cm was 44.2%, and the ratio of Part 3 to the whole number of bars was 17.4%. The ratio of Part 1 to the total number of steel bars with a length larger than 100 cm was 15.4%, and the ratio of Part 3 to the whole number of bars was 23.9%. In both situations, the maximum percentage of steel bar length was 61 to 80 cm.

It was found that when the steel bar with a diameter of 16 mm was cut, the disc cutter had a better cutting effect when the penetration depth was small. The long steel bar still accounted for a large proportion because the effect of cutter cutting concrete was good and obvious. The concrete on the palm surface was crushed, and the steel mesh was exposed to the surface. The longer steel bars discharged from the cutterhead's edge as it rotated because there was no seal between the working face of the test platform and the cutterhead.

In actual engineering, the large diameter steel bars will be attached to the cutterhead and further rolled by the disc cutter or wound around the cutterhead.

4. Numerical Models

Disc cutter cutting the reinforced concrete diaphragm wall is a complex dynamic cutting process. In order to simplify the model and more thoroughly analyze the link between the disc cutter blade and reinforced concrete, we built a three-dimensional model of a disc cutter cutting reinforced concrete through using a numerical simulation method and examined the effects of varied penetration depths and cutter spacing.

4.1. Numerical Model of Disc Cutter Cutting

A fully functional explicit dynamic analysis finite element software ANSYS/LS-DYNA was used to establish a three-dimensional linear cutting model of reinforced concrete members and disc cutters, as shown in Figure 9. Reinforcement and concrete were modeled by the common node method, and solid hexahedral elements were used. The concrete material was the No. 272 RHT model, and the steel bar was made of No.3 *MAT-PLASTIC-KINEMATIC. The diameter of the cutter was 432 mm, and the blade width was 14 mm. Without considering the wear of the disc cutter, the knife ring was set as a rigid body, and the solid tetrahedral unit was adopted. The main parameters of model materials are shown in Table 5. Considering the size effect of the structure, the simulation results show that when the model size of the reinforced concrete member was $650 \times 250 \times 50$ mm, the average cutting force difference of the disc cutter compared with the previous size was less than 5%, which was considered to be less affected by the model size. The diameter of the steel bar was 25 mm. The thickness of concrete cover from the reinforcement bar was 15 mm. The mesh of the reinforced concrete layer was encrypted, and the total grid number of the model was 84,657.

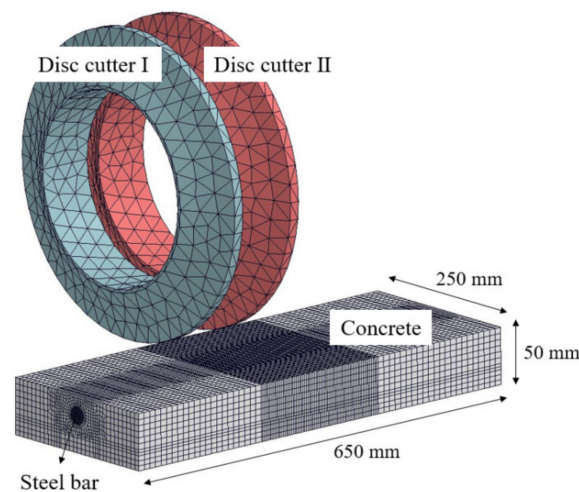


Figure 9. Three-dimensional numerical model.

Table 5. Main parameters of model material.

Object	Material	Parameter	Value	Parameter	Value	Parameter	Value	
Disc cutter	Rigid	Mass density	8.0 g/cm ³	Young's modulus	210 GPa	Poisson's ratio	0.25	
		Concrete	RHT	Mass density	2.3 g/cm ³	Elastic shear modulus	16.7 GPa	Parameter for polynomial EOS B0
			Parameter for polynomial EOS B1	1.22	Parameter for polynomial EOS T1	35.27 GPa	Failure surface parameter A	1.92
			Failure surface parameter N	0.76	Compressive strength	0.05 GPa	Relative shear strength	0.18
			Relative tensile strength	0.1	Lode angle dependence factor	0.69	Lode angle dependence factor	0.0048
Steel	Plastic	Mass density	7.6 g/cm ³	Young's modulus	210 GPa	Poisson's ratio	0.29	
		Yield stress	0.586 GPa	Tangent modulus	1.1 GPa	Failure strain for eroding elements	0.1	

The bottom nodes of the concrete member constrained the displacement and rotation in each direction, and the surrounding nodes were given non-reflective boundary conditions. The contact between the cutter and reinforced concrete adopted surface-to-surface erosion contact. The cutter had three directions of motion in this model. The shield cutterhead rotated at a rate of 2 r/min, and the cutter cut at a speed of 0.3 m/s. The cutter also rotated around its own central axis and had a fixed cutting depth each time.

4.2. Dynamic Response of Disc Cutter under Different Penetration Depths

The distance between the two disc cutters was 100 mm, and the penetration degree of disc cutters was set at $P = 3 \text{ mm/r}$, 5 mm/r , 10 mm/r , 15 mm/r , and 20 mm/r . The disc cutter cut the reinforced concrete members back and forth until the reinforcement broke, and the simulation effect is shown in Figure 10.

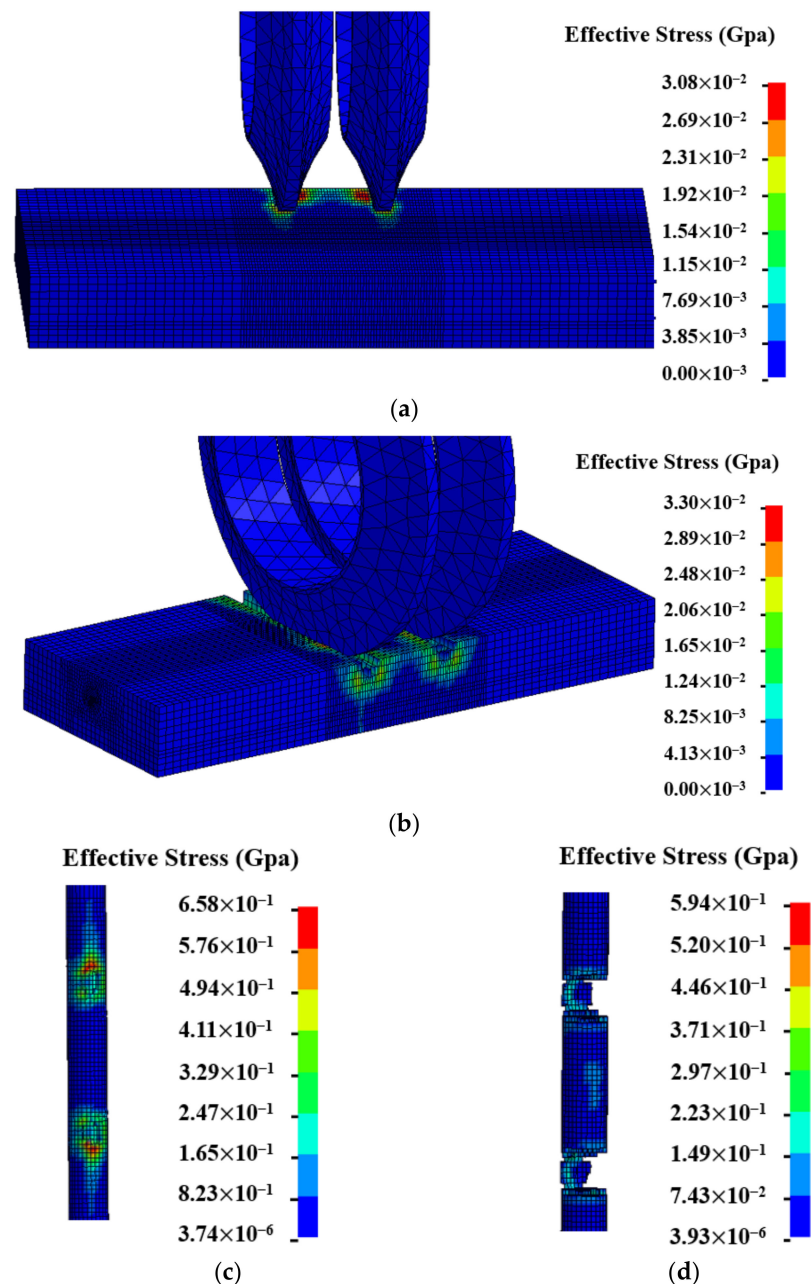


Figure 10. Simulation of reinforced concrete structure breaking by two disc cutters. (a) effective stress when concrete is cut firstly; (b) effective stress during the stage of stable cutting; (c) effective stress when the steel bar is cut firstly; (d) effective stress when the steel bar is about to break.

The disc cutter first made contact with the concrete's surface as the cutting process moved forward, as shown in Figure 10a. At the same time, the concrete under the disc cutter had a large stress due to rolling. When the cutting depth reached a stable value, two grooves were cut out of the concrete, and the equivalent stress of the concrete between the two disc cutters was penetrated, as shown in Figure 10b. When the cutter contacted the steel bar, stress concentration appeared in the contact area, and when the stress reached the failure stress, incision was generated, as shown in Figure 10c. Figure 10d depicts the bar's final fracture.

Through evaluating the effectiveness of a disc cutter cutting reinforced concrete structures, the load of the cutter is crucial. The whole stable section of the cutting process was taken to remove the force data of the disc cutter cutting element concrete layer. The average value and maximum peak value of vertical force and rolling force of disc cutters cutting a reinforced concrete structure under different penetration degrees were calculated, as shown in Table 6. λ represents the ratio between the peak value of the disc cutter force and the average value, reflecting the degree of cutting stability.

Table 6. Data of disc cutter force with different penetration depths.

Penetration Depth/(mm/r)	Normal Force/(kN)		λ	Rolling Force/(kN)		λ
	Mean	Maximum		Mean	Maximum	
3	153.1	260.3	1.7	10.9	17.4	1.6
5	159.7	255.5	1.6	11.3	17.5	1.5
10	174.6	314.3	1.8	12.2	21.4	1.8
15	191.5	363.9	1.9	13.2	28.9	2.2
20	208.5	437.9	2.1	14.3	34.1	2.4

λ = maximum/mean.

The research found the following: (1) The mean of the normal force and rolling force of the disc cutter was positively correlated with the penetration depth. The growth rate of normal force was larger than the rolling force. (2) As the penetration depth increased, λ also increased accordingly. This shows that the larger the penetration depth, the more unstable the disc cutter load. When the penetration depth was larger than 10 mm/r, the rolling force λ was greater than the normal force. At this time, the cutterhead was prone to excessive torque.

The normal force of the test disc cutter in Part 2 of the test was taken as the same as that in the simulation for comparative analysis. Figure 11 depicts the normal force scatter diagram that corresponded to the real-time penetration depth feedback value during the test disc cutter's cutting process. In order to make the data more effective, the mean and standard deviation control charts were introduced to discharge the sensor abnormal data. According to the data points in the (Mean + Standard deviation–Mean–Standard deviation) range, the test disc cutter penetration depth feedback value was primarily concentrated near 30 mm/r, as indicated in the blue area of Figure 12.

The blue triangle scatter data in Figure 12 displays the mean of each penetration depth for the blue area data points. The test feedback penetration was nearly linear with the normal force of the disc cutter, according to the regression analysis of the data points. Figure 12 shows that the correlation between the penetration depth and the cutter's normal force was consistent with the trend of the experimental result. The numerical sample range was centered at the location where the disc cutter touched the steel bar, and the experimental value disc cutter contacted the pure concrete for a longer period of time. In summary, the normal force simulation value was higher than the experimental value.

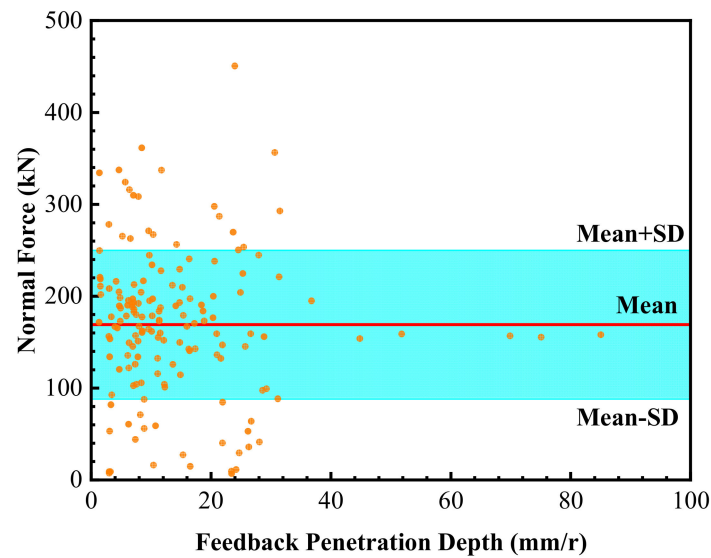


Figure 11. Feedback value of the penetration depth of the test disc cutter and the scatter diagram of normal force.

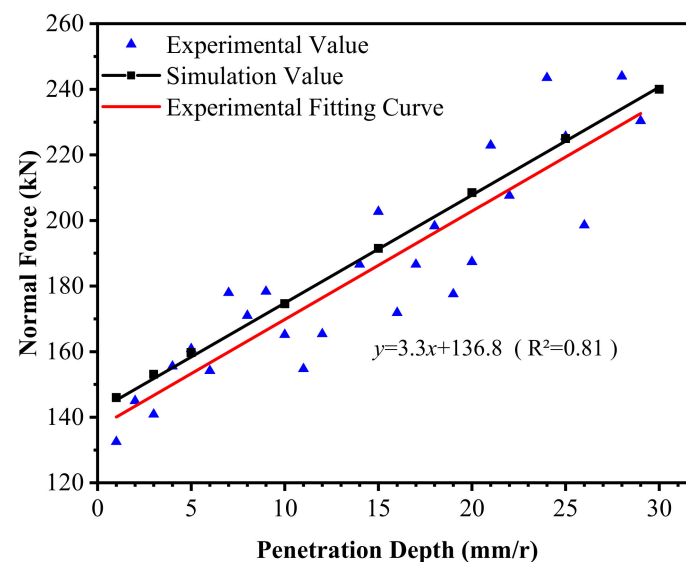


Figure 12. Comparison of numerical and experimental values of the normal force of a disc cutter.

4.3. Effect of Cutter Spacing on the Cutting Performance of a Disc Cutter

Cutting spacing is an important research content of tool head configuration and a direct factor affecting the cutting efficiency of the shield. A disc cutter is used to cut hard rock, and the cutter can avoid producing a concrete backbone. Experiments show that disc cutter cutting concrete has high efficiency. When the cutter space is 100 mm, the concrete between the cutter spacing can be penetrated. In order for the steel bar to discharge from the screw conveyor, the cutter spacing setting for reinforced concrete must also minimize the cutting length of the steel bar while still meeting the requirements for cutting concrete.

For practical engineering, the cutter spacing is generally between 80 and 120 mm. In the case of the same penetration depth ($P = 5 \text{ mm/r}$), three cutter spacings of 80 mm, 100 mm, and 120 mm were numerically simulated. The effective stress of one-time cutting of a steel bar under different cutter spacings is shown in Figure 13. The results show that the equivalent stress zones caused by the two disc cutters were relatively independent, and the equivalent stress of the steel bar was mainly located in the vertical direction with little difference in stress values. Therefore, the cutter spacing had little effect on the cutting

length of the steel bar. For the whole disc cutter cutting reinforced concrete structure, the cutter spacing should be comprehensively determined by the cutter box size, the disc cutter size, and the cutterhead structure.

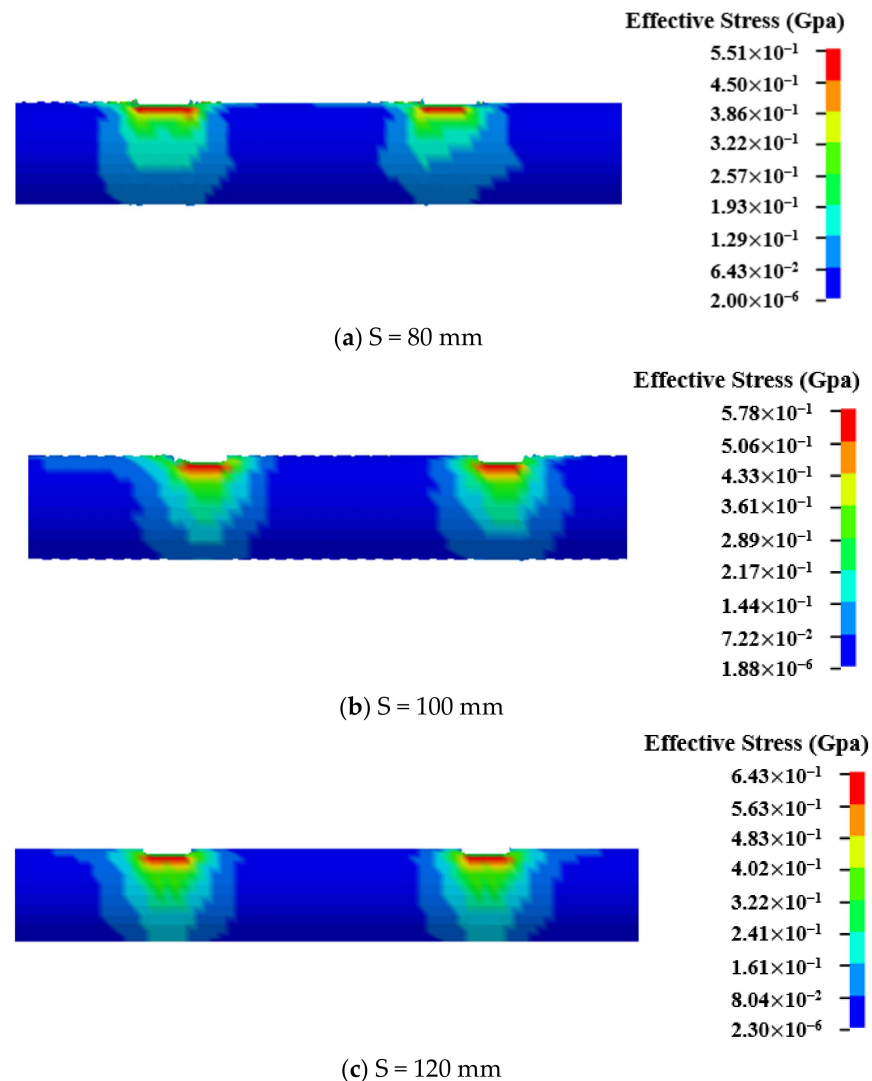


Figure 13. Effective stress of steel reinforcement under different cutter spacings.

5. Conclusions

Through the tunneling test and numerical simulation of reinforced concrete ground wall cutting with a full disc cutter, the feasibility of using a full cutter head to cut a reinforced concrete ground wall is proven. The adaptability of the disc cutter cutting a reinforced concrete ground wall was analyzed from the angle of cutter spacing, driving parameters, and test response, and the conclusions are as follows:

Firstly, it is possible to design a reinforced concrete diaphragm wall that a disc cutter cuts. The benefit of using a disc cutter to cut reinforced concrete diaphragm walls is that the shield tunneling torque is minimal, the cutting efficiency is excellent, and the environmental effect is minimized. If the driving parameters are not properly controlled, the cutting steel bar will be too long.

Secondly, the low penetration depth should be adopted when the disc cutter is cutting the reinforced concrete diaphragm wall, and the penetration depth is recommended to be controlled within the range of 10 mm/r. The cutterhead speed and thrust should be controlled to ensure that the torque is in a small floating range. The test results show that the fracture caused by disc cutter cutting steel bars can be divided into single-sided

rolling failure, double-sided rolling failure, and brittle failure. When the steel bar was well constrained, the disc cutter was able to effectively cut the steel bar. When driving settings were carefully managed, the percentage of steel bars less than 60 cm in length was able to increase to 44.2%.

Finally, the simulation results show that the larger the penetration degree, the more unstable the disc cutter load. The trend of the simulated cutter vertical force was consistent with the experimental value, which verified the rationality of the model. When the cutter spacing was more than 80 mm, the cutter spacing had little effect on the cutting results of steel bars.

Author Contributions: Conceptualization, H.Y. and L.C.; methodology, H.Y. and L.C.; software, H.Y.; validation, H.Y., L.C. and K.P.; formal analysis, H.Y.; investigation, L.C.; resources, L.C.; data curation, K.P.; writing—original draft preparation, H.Y.; writing—review and editing, H.Y.; visualization, L.C.; supervision, L.C.; project administration, L.C.; funding acquisition, L.C. All authors have read and agreed to the published version of the manuscript.

Funding: This research received no external funding.

Institutional Review Board Statement: Not applicable.

Informed Consent Statement: Not applicable.

Data Availability Statement: Not applicable.

Conflicts of Interest: The authors declare no conflict of interest.

References

1. Rajak, D.K.; Wagh, P.H.; Linul, E. Manufacturing technologies of carbon/glass fiber-reinforced polymer composites and their properties: A review. *Polymers* **2021**, *13*, 3721. [\[CrossRef\]](#)
2. Wu, G.; Jia, S.; Chen, W.; Yang, J.; Yuan, J. Modelling analysis of the influence of shield crossing on deformation and force in a large diaphragm wall. *Tunn. Undergr. Space Technol.* **2018**, *72*, 154–161. [\[CrossRef\]](#)
3. Huang, R.; Hu, J.; Pan, J.; Wu, Y.; Ren, X.; Zeng, D.; Wang, Z.; Wang, S. The II-Formed Diaphragm Wall Construction for Departure and Reception of Shield Machine. *Sustainability* **2022**, *14*, 7653. [\[CrossRef\]](#)
4. Nematollahi, M.; Dias, D. Interaction between an underground parking and twin tunnels—Case of the Shiraz subway line. *Tunn. Undergr. Space Technol.* **2020**, *95*, 103150. [\[CrossRef\]](#)
5. Wang, Y.; Wang, X.; Xiong, Y.; Yang, Z.; Zhang, J. Full-Scale Laboratory Test of Cutting Large-Diameter Piles Directly by Shield Cutterhead. *Adv. Civ. Eng.* **2022**, *2022*, 8780927. [\[CrossRef\]](#)
6. Liu, B.; Li, T.; Han, Y.; He, Y.; Fu, C. The problem of wedge indenter with flat-rounded bottom indenting half-plane elastic body. *Int. J. Appl. Mech.* **2022**, *14*, 2250010. [\[CrossRef\]](#)
7. Chen, H.; Yuan, D.; Wang, F.; Wang, M. Study on shield cutting parameters when cutting big diameter piles. *China Civ. Eng. J.* **2016**, *49*, 103–109.
8. Li, Z.; Chen, Z.; Wang, L.; Zeng, Z.; Gu, D. Numerical simulation and analysis of the pile underpinning technology used in shield tunnel crossings on bridge pile foundations. *Undergr. Space* **2021**, *6*, 396–408. [\[CrossRef\]](#)
9. Lv, J.; Lin, D.; Wu, W.; Huang, J.; Li, Z.; Fu, H.; Li, H. Mechanical Responses of Slurry Shield Underpassing Existing Bridge Piles in Upper-Soft and Lower-Hard Composite Strata. *Buildings* **2022**, *12*, 1000. [\[CrossRef\]](#)
10. Wang, N.; Jiang, Y.; Geng, D.; Huang, Z.; Ding, H. Numerical Investigation of the Combined Influence of Shield Tunneling and Pile Cutting on Underpinning Piles. *Front. Earth Sci.* **2022**, *10*, 896634. [\[CrossRef\]](#)
11. Liu, B.; Li, T.; Han, Y.; Li, D.; He, L.; Fu, C.; Zhang, G. DEM-continuum mechanics coupling simulation of cutting reinforced concrete pile by shield machine. *Comput. Geotech.* **2022**, *152*, 105036. [\[CrossRef\]](#)
12. Li, X.; Yuan, D.; Jiang, X.; Wang, F. Damages and wear of tungsten carbide-tipped rippers of tunneling machines used to cutting large diameter reinforced concrete piles. *Eng. Fail. Anal.* **2021**, *127*, 105533. [\[CrossRef\]](#)
13. Hu, X.; He, C.; Lai, X.; Walton, G.; Fu, W.; Fang, Y. A DEM-based study of the disturbance in dry sandy ground caused by EPB shield tunneling. *Tunn. Undergr. Space Technol.* **2020**, *101*, 103410. [\[CrossRef\]](#)
14. Yan, L.; Wang, G.; Chen, M.; Yue, K.; Li, Q. Experimental and application study on underpinning engineering of bridge pile foundation. *Adv. Civ. Eng.* **2018**, *2018*, 5758325. [\[CrossRef\]](#)
15. Agrawal, A.K.; Chattopadhyaya, S.; Murthy, V. Delineation of cutter force and cutter wear in different edge configurations of disc cutters—An analysis using discrete element method. *Eng. Fail. Anal.* **2021**, *129*, 105727. [\[CrossRef\]](#)
16. Fang, Y.; Yao, Z.; Xu, W.; Tian, Q.; He, C.; Liu, S. The performance of TBM disc cutter in soft strata: A numerical simulation using the three-dimensional RBD-DEM coupled method. *Eng. Fail. Anal.* **2021**, *119*, 104996. [\[CrossRef\]](#)

17. Tang, S.H.; Zhang, X.P.; Liu, Q.S.; Chen, P.; Sun, X.T.; Sun, L.; Dai, Y.; Chen, S.T. Prediction and analysis of replaceable scraper wear of slurry shield TBM in dense sandy ground: A case study of Sutong GIL Yangtze River Crossing Cable Tunnel. *Tunn. Undergr. Space Technol.* **2020**, *95*, 103090. [[CrossRef](#)]
18. Karami, M.; Zare, S.; Rostami, J. Study of common wear prediction models for hard rock TBM disc cutters and comparison with field observation in Kerman water conveyance tunnel. *Bull. Eng. Geol. Environ.* **2021**, *80*, 1467–1476. [[CrossRef](#)]
19. Lin, L.; Xia, Y.; Mao, Q.; Zhang, X. Experimental study on wear behaviors of TBM disc cutter ring in hard rock conditions. *Tribol. Trans.* **2018**, *61*, 920–929. [[CrossRef](#)]
20. Zhang, X.; Hu, D.; Li, J.; Pan, J.; Xia, Y.; Tian, Y. Investigation of rock breaking mechanism with TBM hob under traditional and free-face condition. *Eng. Fract. Mech.* **2021**, *242*, 107432. [[CrossRef](#)]
21. Munoz, H.; Taheri, A.; Chanda, E. Rock cutting characteristics on soft-to-hard rocks under different cutter inclinations. *J. Rock Mech. Min. Sci.* **2016**, *87*, 85–89. [[CrossRef](#)]
22. Rostami, J. Development of a force Estimation Model for Rock Fragmentation with Disc Cutters through Theoretical Modeling and Physical Measurement of Crushed Zone Pressure. Ph.D. Thesis, Colorado School of Mines, Golden, CO, USA, 1997.
23. Shi, Y.P.; Xia, Y.M.; Tan, Q.; Zhang, Y.C.; Qiao, S. Distribution of contact loads in crushed zone between tunnel boring machine disc cutter and rock. *J. Cent. S. Univ.* **2019**, *26*, 2393–2403. [[CrossRef](#)]
24. She, L.; Zhang, S.R.; Wang, C.; Du, M.; Yang, P. A cutting mechanics model of constant cross-section type disc cutter and its application based on dense core theory. *Int. J. Rock Mech. Min. Sci.* **2022**, *150*, 105025. [[CrossRef](#)]
25. Li, X.; Zhang, Y.; Sun, X. Numerical analysis for rock cutting force prediction in the tunnel boring process. *Int. J. Rock Mech. Min. Sci.* **2021**, *144*, 104696. [[CrossRef](#)]
26. Zhang, Z.; Wang, S.; Huang, X.; Rostami, J. Application of block theory for evaluating face stability under disc cutters loading of TBM, case study of a water-conveyance tunnel project. *Tunn. Undergr. Space Technol.* **2019**, *90*, 249–263. [[CrossRef](#)]
27. Liu, W.; Ding, L. Global sensitivity analysis of influential parameters for excavation stability of metro tunnel. *Autom. Constr.* **2020**, *113*, 103080. [[CrossRef](#)]
28. Liu, B.; Wang, Y.; Zhao, G.; Yang, B.; Wang, R.; Huang, D.; Xiang, B. Intelligent decision method for main control parameters of tunnel boring machine based on multi-objective optimization of excavation efficiency and cost. *Tunn. Undergr. Space Technol.* **2021**, *116*, 104054. [[CrossRef](#)]
29. Faramarzi, L.; Kheradmandian, A.; Azhari, A. Evaluation and optimization of the effective parameters on the shield TBM performance: Torque and thrust—Using discrete element method (DEM). *Geotech. Geol. Eng.* **2020**, *38*, 2745–2759. [[CrossRef](#)]
30. Lyu, H.M.; Shen, S.L.; Zhou, A.; Yin, Z.Y. Assessment of safety status of shield tunnelling using operational parameters with enhanced SPA. *Tunn. Undergr. Space Technol.* **2022**, *123*, 104428. [[CrossRef](#)]